Journal of Sol-Gel Science and Technology (2021) 99:376–390
https://doi.org/10.1007/s10971-021-05580-4

ORIGINAL PAPER: SOL–GEL AND HYBRID MATERIALS FOR CATALYTIC, PHOTOELECTROCHEMICAL AND SENSOR APPLICATIONS

Characterization and catalytic reactivity of xerogel catalysts based on mesoporous zirconia doped with telluric acid prepared by sol–gel method: mechanistic study of acetic acid esterification with benzyl alcohol

Wafa Ksila[1,2] · Mohamed Kadri Younes[1] · Abdelhamid Ghorbel[1] · Alain Rives[2]

Received: 6 February 2021 / Accepted: 18 June 2021 / Published online: 8 July 2021

Abstract

Our work is focused on the research of new zirconia doped telluric acid catalysts prepared with sol–gel method. Optimization of different preparation parameters of the catalyst, such as the HNO_3 assisted synthesis, molar ratio $nTe(OH)_6$/nZr, and calcination temperature, was studied. Catalysts were characterized by N_2-physisorption at 77 K, X-ray diffraction, UV–Vis spectroscopy, X-ray photoelectron spectroscopy (XPS), Electron Scanning Microscopy, and surface acidity titration. The catalytic activity was tested in the esterification reaction of benzyl alcohol with acetic acid. The addition of HNO_3 in the gelling step greatly improves the acidity of the catalyst through the development of the texture. Doping of zirconia by telluric acid improves the acidity of the catalyst and the catalytic performance, but this improvement does not follow the increase in the quantity of the doping agent in the catalyst. However, calcination of the catalyst allows the development of tetragonal ZrO_2 phase and causes a loss in acidity and consequently a decrease in catalytic activity. Kinetics and mechanism study indicates that the catalytic reaction is of first order and is by the Eley–Rideal mechanism in which the adsorbed acetic acid species react with benzyl alcohol in the fluid phase to form the corresponding ester. By the application of Eyring's theory shows that the adsorption step is endothermic and that a fast associative mechanism occurs between the adsorbed species and the second reagent.

Graphical Abstract

The correlation between catalytic activity, surface acidity and catalysts morphology.

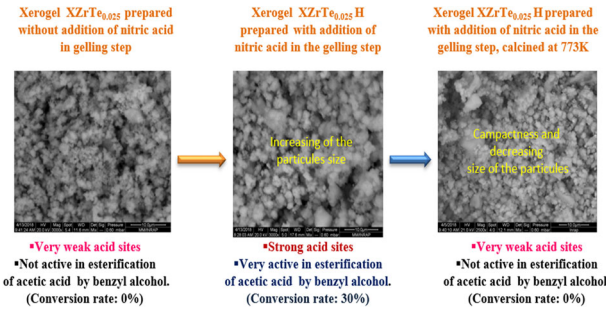

✉ Wafa Ksila
Wafa.ksila@univ-lille.fr

[1] Faculté des Sciences de Tunis, Université de Tunis El Manar, LR01ES08 Chimie des Matériaux et Catalyse, 2092 Tunis, Tunisie

[2] Univ. Lille, CNRS, Centrale Lille, ENSCL, Univ. Artois, UMR 8181 - UCCS - Unité de Catalyse et Chimie du Solide, F-59000 Lille, France

Keywords Sol–gel · Zirconia · Telluric acid · Nitric acid · Surface acidity · Esterification · Acetic acid

Highlights

- Preparation of new telluric acid doped zirconia by sol–gel process with nitric acid allows the development of new ZrTe phase.
- The addition of nitric acid in the gelling step has a great effect on the textural, morphology and acidity properties of catalysts. Consequently, their reactivity is improved.
- Kinetic studies have shown that esterification of benzyl alcohol with acetic acid follows an Eley–Rideal mechanism with a first order.

1 Introduction

Growing concerns about environmental pollution and the depletion of fossil fuel reserves have inspired research into clean and renewable sources of energy to meet both environmental and energy challenges. Among these resources, fuel additives are one of the main alternatives to energy problems and contribute to the reduction of exhaust emissions of pollutants, in particular fine particles, carbon monoxide, sulfur oxides, and nitrogen oxides [1]. The synthesis of fuel additives is based on esterification [2] and transesterification [3] reactions in the presence of acid catalysts. However, these catalysts must not have any impact on the environment.

Esterification reactions are an important route for the synthesis of esters used in many chemical industries such as biodiesels, drugs, plasticizers, food preservations, pharmaceuticals, solvents, perfumes, cosmetics, and chiral auxiliaries [4, 5]. Current practice requires the use of Lewis or mineral acids in homogeneous catalysis, but this process is usually accompanied by the production of a substantial amount of waste and high corrosion [6]. To avoid these problems, the use of solid acids such as zeolite [7] or modified metal oxides [8] is convenient and effective for acid-catalyzed esterification reactions.

Zirconium oxide is an important material for many industrial applications. It has high thermal stability under different conditions and has a surface with acid–base sites [9–12]. Its modification by the addition of oxoanions such as SO_4^{2-} or PO_4^{3-} affords more stability, inhibits sintering, and gives the catalysts a suitable surface acidity for many reactions [13–17].

The kinetics and mechanistic study of catalyzed esterification have shown that the results differ from one study to another. The Langmuir–Hinshelwood (LH) and Eley–Rideal (ER) models are commonly used to correlate kinetic data for esterification reactions catalyzed by solid acids [18–21].

To modify texture and acidity of zirconia by other doping agent we present in this work the preparation by sol–gel route and the optimization of some preparation parameters of xerogel catalysts based on zirconia doped by telluric acid such us the effect of the addition of nitric acid in the gelling step, doping agent content and the calcination temperature. This parameter optimization is applied in the reaction of esterification of acetic acid by benzyl alcohol chosen as test reaction. To propose a mechanism for the reaction, ER and LH mechanisms were confronted to kinetic results of acetic acid esterification with benzyl alcohol over the catalyst which presents the best catalytic performances. Enthalpy adsorption step and thermodynamics activation parameters were also determined using Eyring extended theory.

2 Experimental

2.1 Catalyst preparation

Zirconia xerogel doped telluric acid catalysts were prepared by sol–gel route in the absence and in the presence of nitric acid at the gellification step. In the first step, zirconium (IV) butoxide (Aldrich 80% in 1-butanol) was dissolved in 1-butanol. The mixture is then stirred for 30 min. After that, the nitric acid is added if necessary in the n_{HNO3}/n_{Zr} ratio equal 0.5. After stirring for 1 h, the hydrolysis is carried out by the dropwise addition of distilled water (hydrolysis ratio $n_{H2O}/n_{Zr} = 3$) and the mixture is stirred at room temperature until the formation of the gel. For doped catalysts, telluric acid (Merck, 99%) was dissolved in the distilled hydrolysis water with different molar ratios ($n_{Te}/n_{Zr} = 0.025$; 0.05; 0.1). After complete formation, the gel was dried in an oven under ordinary conditions ($P = 1$ bar, $T = 393$ K) for 24 h.

To study the effect of the calcination temperature on the characteristics and the reactivity of the catalysts after the drying step, the materials are calcined under pure oxygen (flow rate $= 30\ cm^3\ min^{-1}$) at 573 and 773 K (temperature ramp: $1\ K\ min^{-1}$; temperature step: 3 h).

The prepared catalysts are named as follow $XZrTe_xHT$, with X: xerogel; Zr: zirconium; Te: telluric acid; x: (nTe/nZr)*100; H: Nitric acid; T: calcination temperature. Designation of prepared catalysts is given in Table 1.

Table 1 Designation and chemical composition of prepared xerogel catalysts

Catalyst	*HNO₃/Zr*[a]	Te/Zr[a]	Te/Zr[b]	O/Zr[b]	C/Zr[b]	Calcination temperature (K)
XZrH	0.5	0				–
$XZrTe_{2.5}$	0	0.025	0.04	2	1.3	–
$XZrTe_{2.5}H$	0.5	0.025	0.05	2.3	1.7	–
$XZrTe_{2.5}H$ 773	0.5	0.025	0.05	2.3	1.7	773
$XZrTe_5H$	0.5	0.05				–
$XZrTe_{10}H$	0.5	0.1	0.16	2.8	1.6	–

[a]Theoretical atomic ratio

[b]Atomic ratio obtained by EDX

2.2 Characterization techniques

SEM FEI-quanta 200 Scanning Electron Microscope was used to obtain images and morphologies of the catalysts. Elemental analysis was obtained by Energy Dispersive X-ray Analysis (EDX) detector.

N_2-adsorption-desorption isotherms at 77 K were performed with a Micromeritics ASAP 2020 apparatus after outgassing the catalyst at 573 K for 3 h. The specific surface area and pore size distribution were determined by BET and BJH methods, respectively.

UV–Vis spectra were recorded on a Perkin Elmer spectrophotometer type Instrument (Lambda 650 s UV/Vis spectrometer) equipped with an integrating sphere. The apparatus consists of a double beam and a double monochromator. The sources used are of the tungsten-halogen and deuterium types. The range of wavelengths analyzed extends from 190 to 900 nm. The solids are analyzed in the form of ground powder as finely as possible. The spectra of the solid samples were recorded between 200 and 900 nm with a 0.2 nm pitch.

XRD patterns were recorded on a powder PANalytical X'Pert PRO diffractometer using a CuK_α radiation ($\lambda = 1.54$ Å). The diffractograms were recorded for the incident angle of 2θ values between 3° and 70° with a scanning speed of $0.02° s^{-1}$.

The analyses XPS were performed using a photoelectron X Kratos AXIS Ultra DLD spectrometer equipped with an Al monochromatic Kα source ($h\nu = 1486.6$ eV) for pressures below 10^{-9} Pa. The CasaXPS software was used to process the spectra obtained after analysis. The spectral decomposition are performed according to the Lorentz/Gaussian model after calibration of the peaks of each element with respect to that of C1s at 284.6 eV.

Qualitative surface acidity of catalysts was studied by the adsorption of the Hammett indicators. The method consists in putting the solid in the form of a suspension in a non-polar solvent containing the color indicator of known pKa and observing the color obtained. If the color is that of the acid form of the indicator, the value of the Hammett function Ho of the surface is lower than the pKa of the indicator. The use of several indicators allows surrounding the value of H_0 greatness.

Strength and quantity of surface acidity of the prepared catalysts were measured using a potentiometric titration method [22–24]. This method consists in stirring a suspension of 50 mg of solid in 90 mL of acetonitrile for 3 h. The suspension was titrated with a 0.05 mol/L solution of n-butylamine in acetonitrile. The potential variation was measured with an Adwa (AD1000) pH-potentiometer.

2.3 Catalytic test

To study the catalytic properties of the catalysts for esterification reaction of acetic acid with benzyl alcohol, 200 mg of the catalyst was introduced into a two-necked flask with a reaction mixture which is composed of 10 mL ($9.64\ 10^{-2}$ mol) of benzyl alcohol and 1 mL ($1.66\ 10^{-2}$ mol) of acetic acid. These were added using a graduated pipette. The reaction mixture was maintained at 353 K, throughout the reaction, under reflux. Acetic acid in reaction medium was titrated at different time using pH-metric method titration.

The mechanistic study of the esterification reaction is based on the determination of the rate of the reaction for different concentrations of acetic acid while keeping that of benzyl alcohol constant. The reaction is carried out under reflux, in a two-necked flask, placed in an oil bath at a temperature set at 353 K. A mass of 200 mg of the catalyst $XZrTe_{2.5}H$, is introduced into the flask. The reaction mixture consists of benzyl alcohol with a fixed concentration of $1\ mol\ L^{-1}$ and acetic acid, the concentration of which varies according to the ratios $C_A/C_{AB} = 1$; 1/2; 1/3; 1/4. Toluene is used as solvent. The acetic acid conversion is determined with sodium hydroxide at a concentration of $0.05\ mol\ L^{-1}$, in the presence of phenolphthalein used as a color indicator to determine the point of equivalence.

3 Results and discussion

3.1 Elemental analysis

Elemental chemical analysis of xerogels $XZrTe_{2.5}$, $XZrTe_{2.5}H$, and $XZrTe_{10}H$ catalysts are presented in

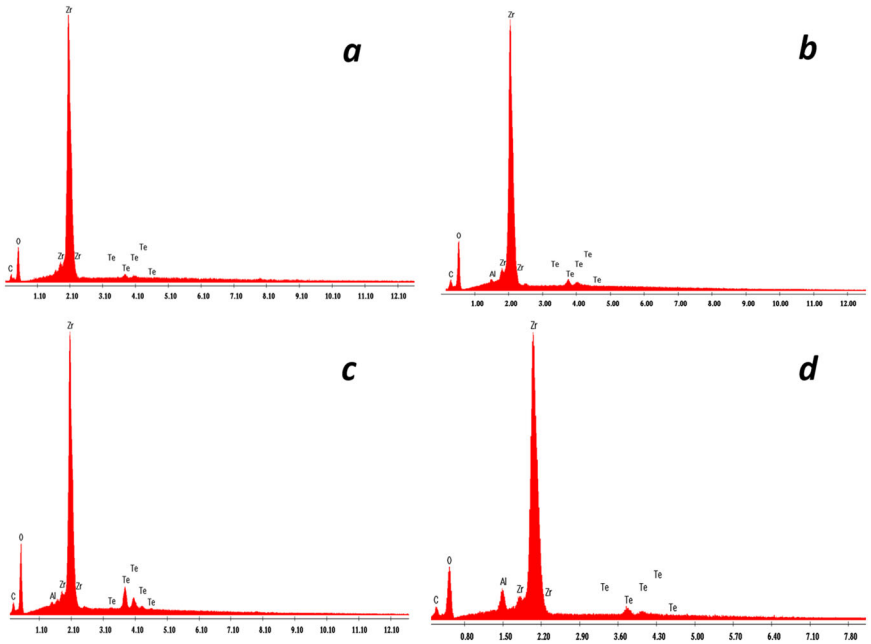

Fig. 1 Elemental chemical analysis of xerogel $XZrTe_{2.5}$ (**a**), $XZrTe_{2.5}H$ (**b**), $XZrTe_{10}H$ (**c**) and $XZrTe_{2.5}H773$ (**d**) catalysts

(Fig. 1a–c). It confirms the presence of tellurium in the catalysts. The doping with telluric acid from the atomic ratio 0.025–0.1 causes the increase of the intensity of the energy of transition of tellurium. Quantitative analysis of the samples is presented in Table 1. The results show that the atomic ratio (Te/Zr) practically doubles with respect of the theoretical value.

3.2 Morphology of catalysts

The scanning electron microscopy images of catalysts are presented in Fig. 2. Images of $XZrTe_{2.5}$ and $XZrTe_{2.5}H$, after drying at 393 K (Fig. 2a, b respectively), show that these catalysts are characterized by spherical aggregates with heterogeneity. The size of particles increases from 2 to 4 µm by adding nitric acid in the gelling step.

SEM micrograph of $XZrTe_{10}H$ catalyst is shown in Fig. 2c. Its morphology is also characterized by spherical aggregates. In comparison with the $XZrTe_{2.5}H$ catalyst (Fig. 2b), aggregates seem to be more compact and smaller with particle size around 1 µm.

The morphology of the $XZrTe_{2.5}H$ catalyst is also modified by calcination at 773 K (Fig. 2d). The particles become more compacted with a size around 2 µm.

3.3 Textural properties

The N_2-adsorption-desorption results of the xerogel catalysts are shown in Fig. 3.

The sample prepared in the absence of nitric acid $XZrTe_{2.5}$ (Fig. 3a) presents an isotherm which is practically of type II according to the IUPAC classification [25] with a very weak hysteresis loop. This indicates that the solid is mainly macroporous which the average pore size is equal to 650 Å.

The Fig. 3b–e show the N_2-adsorption-desorption of $XZrTe_{2.5}H$, $XZrTe_5H$, $XZrTe_{10}H$ and XZrH catalysts respectively. The doping of zirconia with telluric acid prepared in the presence of HNO_3 does not drastically influence the shape of the isotherm comparatively with the catalyst without telluric acid. The observed isotherms are compatible of type IV with the hysteresis loop of the H3 type. This is attributed to open slit-shaped pores observed for non-rigid aggregates or plates-like particles.

The calcination of the $XZrTe_{2.5}H$ catalyst at 773 K leads to a change in the shape of the adsorption isotherm (Fig. 3f).

The textural properties (specific surface, pore volume, and pore distribution) of the catalysts are presented in Table 2.

The pores distribution for $XZrTe_{2.5}$ catalyst reveals the presence of macropores with an average diameter of about 650 Å and confirm the shape of the adsorption curve (Fig. 3a).

The addition of nitric acid and telluric acid in the gelling step has very remarkable effects on the texture of the catalysts such increase of the specific surface and the mesoporous volume and decrease of the macroporosity (Table 2).

In fact, the categories of the pores distribution in the materials are changed, from a bimodal distribution at low loading of telluric acid to a well-defined mesoporous distribution at high loading of telluric acid.

This is may be due to the fact that telluric species reduce the mobility of the grains and prevent the contact between the particles by steric effect of telluric species and

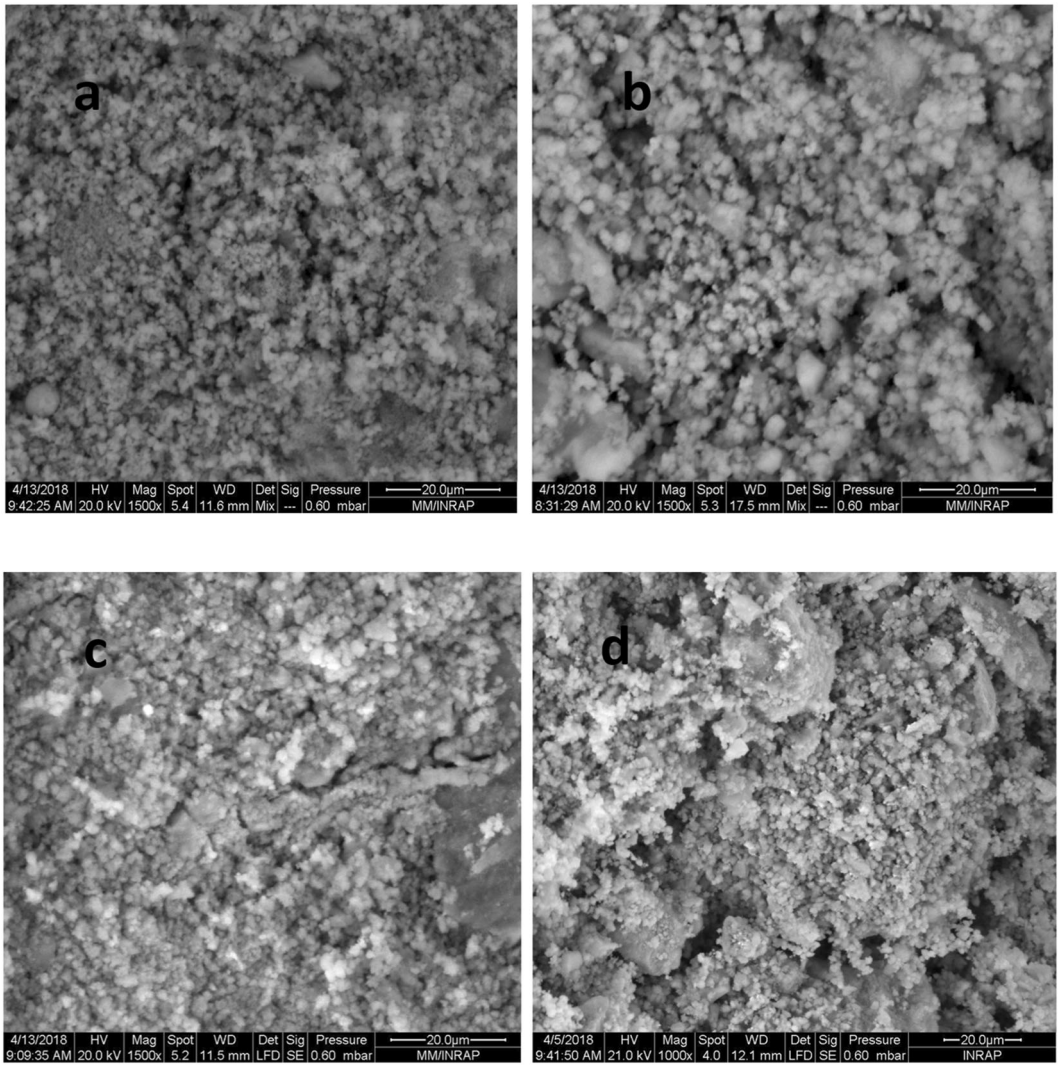

Fig. 2 SEM images of xerogel $XZrTe_{2.5}$ (**a**), $XZrTe_{2.5}H$ (**b**), $XZrTe_{10}H$ (**c**), and $XZrTe_{2.5}H$ 773 (**d**) catalysts

consequently the growth of crystallites is inhibited in a similar manner to that observed upon modifying zirconia with other doping agents [8]. This effect can be explained by the mechanism of the sol–gel process. The structure of a sol–gel material evolves sequentially through successive hydrolysis-condensation reactions. Resulting polymeric structural gels are usually achieved by addition of mineral acids [26, 27] or carboxylic acids [28]. In our case the successive hydrolysis and condensation reactions of butoxide zirconium $(BuO)_4Zr$ precursor can be represented by Scheme 1. Thus resulting dried solids were characterized by a developed texture. In the present case, it seems that the presence of only telluric acid in the solid solution preparation cannot give a sufficient quantity of H^+ to achieve this process of the two reactions and then to obtain polymeric structure in particular by condensation reaction. In fact the medium for solid preparation which does not contain HNO_3 leads to the precipitation reaction of zirconium hydroxide $Zr(OH)_4$ and no gel is obtained even if the reaction mixture is left for a longer time. This shows that the presence of a weak acid can promote hydrolysis, but not enough to induce condensation sufficient to form a gel, while when HNO_3 is added a net gel is formed for a few minutes at room temperature throughout the hole of the volume of the reaction medium.

After calcination at 773 K, a considerable decrease in the surface area and the pore volume is observed with a slight increase in the average pore diameter. This can be associated with the agglomeration of particles by sintering [29].

3.4 UV–Vis spectroscopy study

The UV–Vis spectra of XZrH, $XZrTe_{2.5}$, $XZrTe_{2.5}H$, $XZrTe_5H$ and $XZrTe_{10}H$ are presented in Fig. 4.

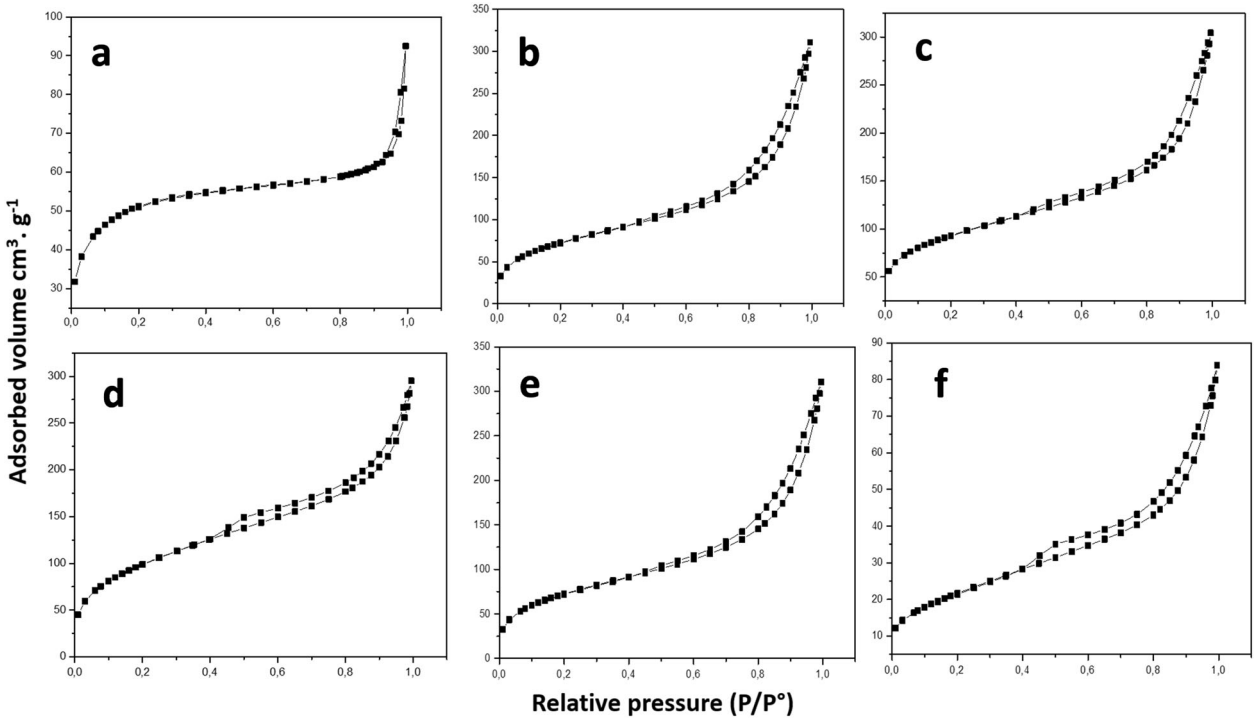

Fig. 3 N_2-adsorption-desorption isotherms of the xerogel, $XZrTe_{2.5}$ (**a**), $XZrTe_{2.5}H$ (**b**), $XZrTe_5H$ (**c**), $XZrTe_{10}H$ (**d**), XZrH (**e**) and $XZrTe_{2.5}H$ 773 (**f**) catalysts

Table 2 Textural properties of xerogel XZrH, $XZrTe_{2.5}$, $XZrTe_{2.5}H$, $XZrTe_5H$, $XZrTe_{10}H$, and $XZrTe_{2.5}H$ 773 catalysts

Catalyst	S_{BET} (m^2/g)	Pore volume (cm^3/g)	Average macroporous size (Å)	Average mesoporous size (Å)
XZrH	271	0.4	130	40
$XZrTe_{2.5}$	179	0.08	650	24
$XZrTe_{2.5}H$	269	0.3	168	44
$XZrTe_5H$	335	0.4	190	40
$XZrTe_{10}H$	369	0.4	190	41
$XZrTe_{2.5}H$ 773	79	0.1	158	32

In general, the UV–Vis absorption of powders based on zirconium oxide is due to charge transfer transitions, corresponding to the excitation of electrons from the O2p valence band to the Zr 4d conduction band ($O^{2-} \rightarrow Zr^{4+}$) and that the coordination of zirconium in oxides varies from six-fold to eight-fold [30]. A band at 256 nm, attributed to the charge transfer with eight-fold coordinated Zr^{4+} [31] is observed for XZrH (Fig. 4a) and for $XZrTe_{2.5}$ (Fig. 4b).

The enrichment of telluric acid from 2.5 to 10 in the sol–gel preparation method causes progressively shift of the band from 268 to 282 nm, indicating the change in coordination state to lower number (Fig. 4c–e). Moreover, a series of bands which extend up to 380 nm is observed. These results are due to the formation of ZrO_2 polymorphs with many defects and low zirconium coordination probably six [32].

3.5 Structural properties

The XRD patterns of $XZrTe_{2.5}$,$XZrTe_{2.5}H$ and $XZrTe_{10}H$ are presented in Fig. 5.

The solids present an amorphous structure with a poorly developed tetragonal [8, 33] ZrO_2 phase characterized by broad peaks, the first is located at 2θ between 19° and 40° and the second at 2θ between 42° and 65° [34, 35].

The addition of HNO_3 in the gelling step causes the decrease of the peak at low angle lower $2\theta = 5°$ which could be due to a change of texture of the solids prepared with nitric acid. Moreover, a new peak located at $2\theta = 12°$ is observed. This is similar to patterns observed with zirconia doped phosphate previously reported [8]. Probably a new ZrTe phase is developed in these conditions.

Comparison of XRD patterns of $XZrTe_{2.5}H$ and $XZrTe_{10}H$ shows that the content of telluric acid does not modify the amorphous texture of the solids.

The diffractograms of XZrH and $XZrTe_{2.5}H$ catalysts calcined at 773 K are presented in (Fig. 6). It shows that heating treatment develops tetragonal phase of ZrO_2 [8, 33], as confirmed by the presence of peaks at $2\theta = 30°$, 35°, 50°, 60° and 62° [34, 35]. Moreover, the peak located at $2\theta = 12°$ (Fig. 6a), attributed in the Fig. 5 to the new ZrTe phase,

Scheme 1 Successive hydrolysis and condensation reactions of zirconium but-oxide $Zr(BuO)_4$ precursor

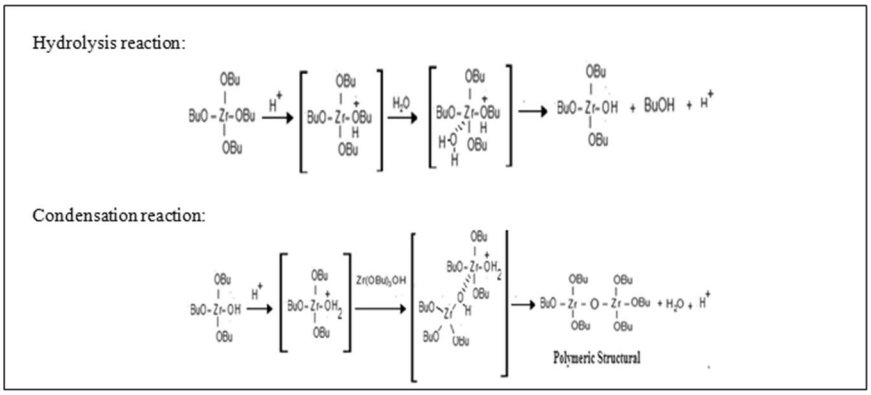

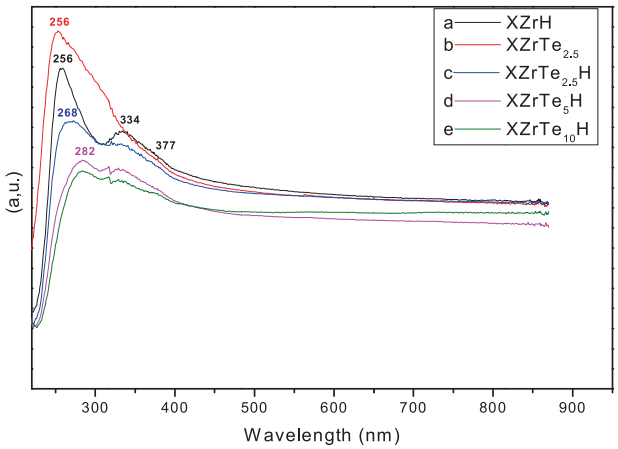

Fig. 4 UV–Vis spectra of xerogel catalysts XZrH, $XZrTe_{2.5}$, $XZrTe_{2.5}H$, $XZrTe_5H$ and $XZrTe_{10}H$

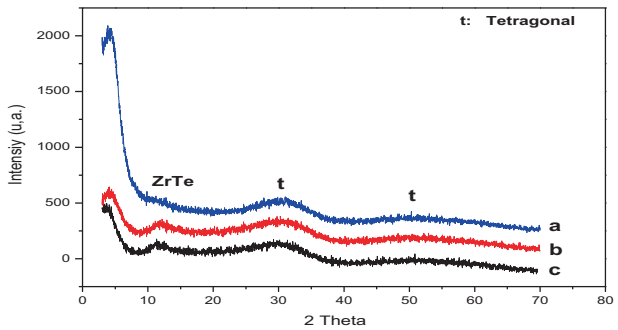

Fig. 5 XRD patterns of xerogel catalysts $XZrTe_{2.5}$ (**a**), $XZrTe_{2.5}H$ (**b**), and $XZrTe_{10}H$ (**c**)

is grown after calcination at 773 K. In reference, the absence of this peak is confirmed on the diffractogram of pure zirconia XZrH calcined at the same temperature (Fig. 6b).

It was already reported that additives such oxoanions [8, 36] or metals [37, 38] to zirconia could stabilize the tetragonal ZrO_2 phase at high calcination temperature. This can be also confirmed when zirconia is doped with telluric

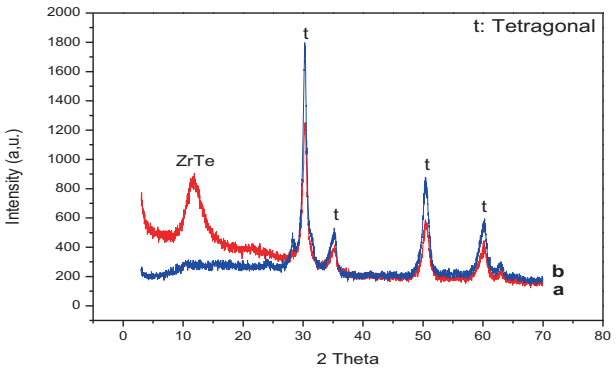

Fig. 6 XRD patterns of xerogel catalysts $XZrTe_{2.5}H$ 773 (**a**) and XZrH 773 (**b**)

acid. The tetragonal ZrO_2 stabilization can be due to a strong surface interaction between ZrO_2 and doping agent, which has a high diffusivity of oxygen due to its anti-Frenkel defect structure [39].

On the other hand, no crystalline phase relative to any tellurium oxide and/or tellurium-zirconium phases were detected, which is probably due to either a low content or a dispersion of the metal on the surface of zirconia.

3.6 X-ray photoelectron spectroscopy (XPS)

The high resolution XPS spectra of Zr 3d, O1s and Te 3d are presented in Figs. 7, 8, 9, and 10a, b for XZrH, $XZrTe_{2.5}H$, $XZrTe_{2.5}H773$, pure telluric acid and telluric acid calcined at 773 K, respectively.

For all catalysts, the C1s peak is due to the adventitious contamination carbon from the organic ligands and solvent. The O1s peak at BE around 530.1 eV could be attributed to the oxygen of ZrO_2 lattice network [39–41]. The O1s peak around 531.5 eV could be attributed to hydroxyl group at the surface of zirconia.

For the XZrH the O1s peak around 533 eV could be attributed to the more acidic hydroxyl group.

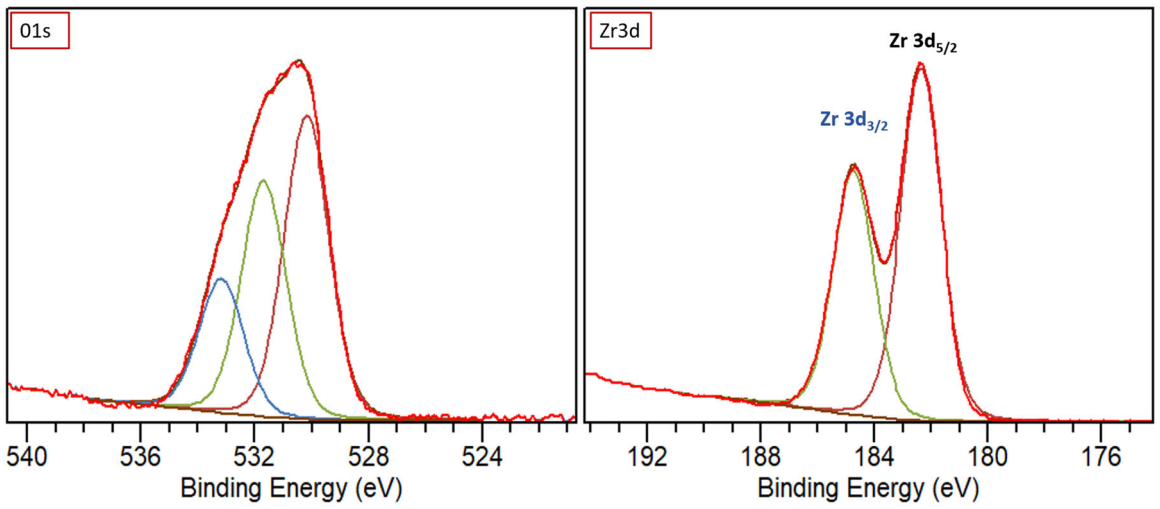

Fig. 7 XPS spectra core level of the XZrH catalyst: O 1s and Zr 3d

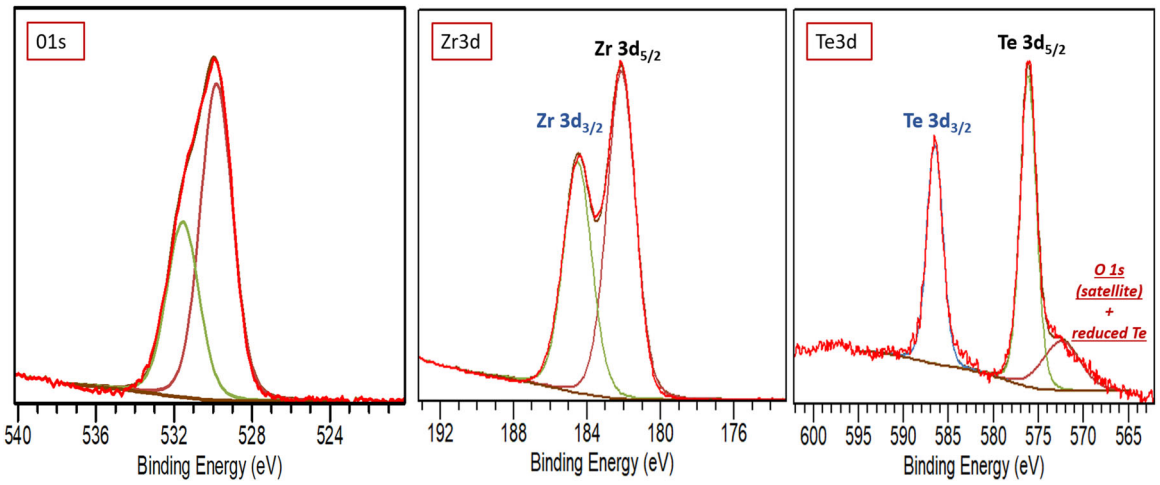

Fig. 8 XPS spectra core level of the $XZrTe_{2.5}H$ catalyst: O 1s, Zr 3d, and Te 3d

This peak decreases drastically for $XZrTe_{2.5}H$, which can be due to the reaction of this species with the $Te(OH)_6$.

The Zr 3d spectrum of XZrH is composed of two simple peaks located at 182.4 eV for Zr $3d_{5/2}$ and 184.7 eV for Zr $3d_{3/2}$ (Fig. 7). These binding energies can be assigned to Zr (IV) oxidation state in ZrO_2 oxide form [40].

The $Zr3d_{5/2}$ peak slightly shift toward lower binding energy at 182.2 eV for the $XZrTe_{2.5}H$ (Fig. 8) due to the interaction between the acidic zirconia and $Te(OH)_6$.

The peak of Te3d could be decomposed in two components $Te3d_{5/2}$ and $Te3d_{3/2}$. For the $XZrTe_{2.5}H$ catalyst, these peaks are located at 576.2 and 586.5 eV respectively (Fig. 8), which could be assigned to Te^{4+} in TeO_2 [41].

The $Te3d_{5/2}$ photopeak for $XZrTe_{2.5}H$ is shifted by 1 eV compared with that of pure telluric acid (Fig. 10a). For $Te(OH)_6$, the $Te3d_{5/2}$ photopeak located at 577.1 eV is assigned to Te^{6+} in TeO_3 or $Te(OH)_6$ [41]. The shift towards the lower binding energy for $XZrTe_{2.5}H$ is due to preparation method which induces a strong interaction of telluric acid with zirconia. This interaction facilitates the formation of TeO_2, compound also observed after calcination of $Te(OH)_6$ at 773 K (Fig. 10b).

After calcination of $XZrTe_{2.5}H$ at 773 K, the observed $Te3d_{5/2}$ and $Te3d_{3/2}$ photopeaks could be divided into two distinct contributions at (573.4; 576.2 eV) and (583.7; 586.6 eV) respectively (Fig. 9). The first peak could be assigned to tellurium in metallic form and the second to TeO_2. The calcination of $XZrTe_{2.5}H$ catalyst leads to a chemical reduction of 25% of the tellurium oxide. For the spectra of catalysts, an additional peak also appears on the lower bonding energies side which could be attributed to an O1s satellite and different bonding states of reduced Te [42]. This result is in agreement with the phase diagram of the Te–O system at 101 kPa that shows the coexistence of metallic

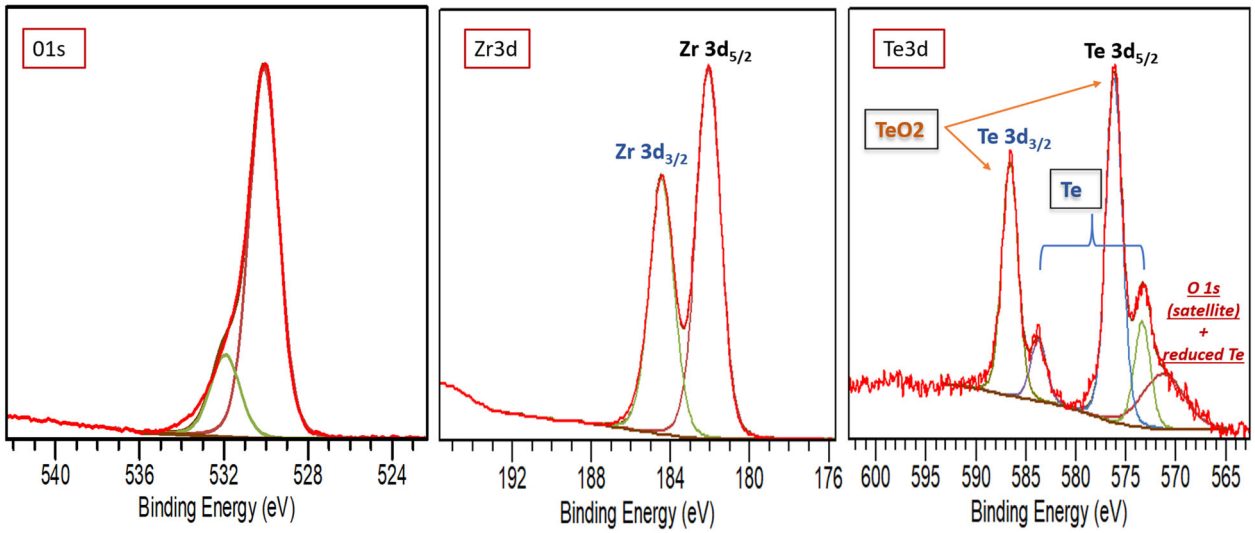

Fig. 9 XPS spectra core level of the $XZrTe_{2.5}H$ 773 catalyst: O 1s, Zr 3d, and Te 3d

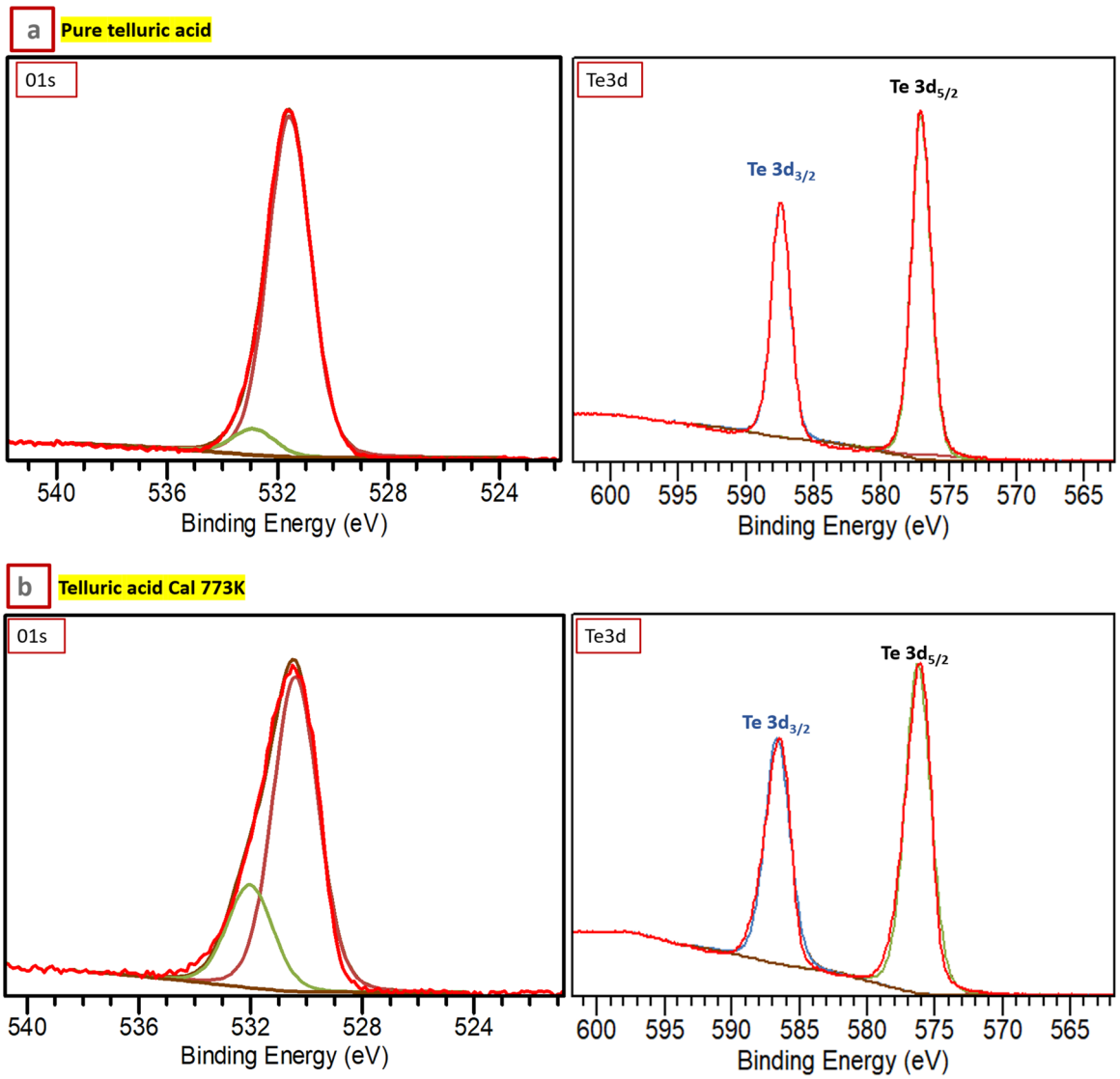

Fig. 10 XPS spectra core level of the pure telluric acid and calcined at 773 K: O 1s and Te 3d

Table 3 The surface atomic compositions of catalysts: the pure zirconium, zirconium dopped with telluric acid, and telluric acid determined by XPS

Catalysts	Atomic ratio Te3d/Zr3d$_{5/2}$	Atomic ratio C1s/Zr3d$_{5/2}$	Atomic ratio O1s/Zr3d$_{5/2}$
XZrH		1.57	2
XZrTe$_{2.5}$H	0.04	1.65	1.81
XZrTe$_{2.5}$H 773	0.04	0.87	1.64
		%At C1s/Te3d$_{5/2}$	%At O1s/Te3d$_{5/2}$
Pure Te(OH)$_6$		3	3.4
Te(OH)$_6$ cal 773		1.3	1.6

tellurium and oxide [43]. The segregation of ZrO_2 and Te was already observed with oxidation of ZrTe alloys [44].

The results (Table 3) show that the atomic ratio (Te3d/Zr3d) practically doubles with respect of the theoretical value, which confirmed the elementary analysis EDX.

3.7 Surface acidity

The acid strength of a solid is the ability of the surface to convert an adsorbed base into its conjugate acid. When the reaction proceeds by proton transfer from the surface to the adsorbate, the acid strength is expressed by Hammett acidity function (Eq. (1)):

$$\mathrm{Ho} = \mathrm{pK}_{\mathrm{BH+/B}} + \log[\mathrm{B}]/[\mathrm{BH}^+] \quad (1)$$

with pK_{BH+} is the ionization constant of the conjugate acid [BH], [BH^+], and [B] are the concentrations of the acid and the base of indicator. By using several indicators with differing pKai values, it is possible to estimate the acid strengths of surface sites. For example, if a solid give color of conjugate acid BH^+ of indicator 1 characterized by pKa1 and show the color of conjugate base of another indicator 2 characterized by pKa2 it can be concluded that the solid surface has acidic sites with H_0 values ranging between pKa1 and pKa2. In our case, purple crystal, methyl red and bromothymol indicators were used for acid strength from $H_0 \leq +7.2$ to $H_0 \leq 0.8$.

The results of the Hammett indicator tests are presented in Fig. 11. They show that the addition of nitric acid in the gelling step improves the acidity of the material. In fact, Hammett function Ho of XZrTe$_{2.5}$ passes from $H_0 > 7.2$ to $0.8 \leq H_0 \leq 4.2$. The qualitative color results of Hammett indicators show that the enrichment of catalysis with telluric acid from 2.5 to 10 does not seem to modify the acidity of the catalyst and H_0 function remains in the range 0.8–4.8. This may indicate that the increase in acidity is due to the more developed Brønsted acidity by the hydroxyl groups following the most important retention of telluric acid in a more developed catalyst texture. However, the calcination of catalysts XZrTe$_{2.5}$H up to 773 K decreases the solid acidity.

To refind this results, the measurement of surface acidity of the solids is carried out by potentiometric titration of n-butylamine in acetonitrile according to the method in [45]. N-butylamine is a strong base and can be adsorbed on acid sites of different strengths and types, thus it titrates both Lewis and Brønsted sites [46]. The acid strength of these sites can be classified according to the following scale [45]: Ei > 100 mV (very strong sites), 0 mV < Ei < 100 mV (strong sites), −100 mV < Ei < 0 mV (weak sites) and Ei < − 100 mV (very weak sites).

The initial electrode potential (Ei) and the calculated amount of the acid sites (mmol/g) of XZrTe$_{2.5}$, XZrTe$_{2.5}$H, XZrTe$_5$H, XZrTe$_{10}$H, and XZrTe$_{2.5}$H773 catalysts which are listed in Table 4. The results reveal that telluric acid doped zirconia passes from a catalyst containing very weak acid sites to one having strong acid sites with increasing acidity amount when nitric acid is added in the gelling step. However, the amount of acid remains practically the same with the enrichment of the catalyst in doping agent. It seems that the weak telluric acid ($pKa_1 = 7.7$; $pKa_2 = 11$) does not change the type of acidity of the catalyst even if its quantity is doubled for the same loading. The initial potential and the amount of the surface acidity show that the type of acidity has not changed, the catalyst contains always strong acid sites but the initial potential decreases, reflecting that the mean strength of the acid sites of catalyst varies.

According to the results of the characterization which show an important change in the texture and the structure of catalyst as well as the loss of the doping agent and OH hydroxyl groups, the decrease in the acidity of the catalyst is evident. Indeed the strength of the catalyst acidity and the total number of acid sites determined by potentiometric titration method decrease dramatically when the catalyst is calcined at 773 K.

3.8 Catalytic properties

Catalytic properties presented in Table 4 show that the addition of nitric acid in gelling step leads to an increase in conversion rate of acetic acid esterification reaction by benzyl alcohol. On the basis of the development of the texture and the increase in the acidity of the catalyst, the

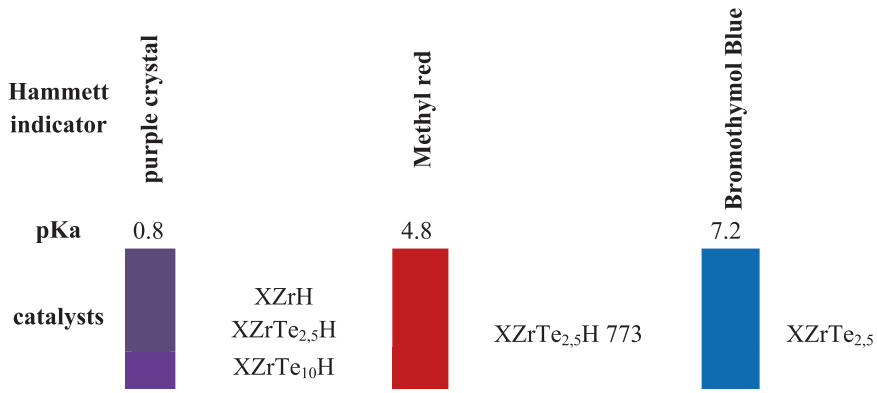

Fig. 11 Hammett indicators tests of surface acidity of xerogel XZrH, $XZrTe_{2.5}$, $XZrTe_{2.5}H$, $XZrTe_5H$, $XZrTe_{10}H$, and $XZrTe_{2.5}H$ 773 catalysts

Table 4 Qualitative and quantitative surface acidity and initial rate of xerogel $XZrTe_{2.5}$, XZrH, $XZrTe_{2.5}H$, $XZrTe_5H$, $XZrTe_{10}H$, and $XZrTe_{2.5}H$ 773 catalysts

Catalysts	Ei (mV)	Acid amount (mmol/g)/ µmol/m^2	%Conv For 4 h
$XZrTe_{2.5}$	−130	0.6 /3.4	0
XZrH	80	0.7/2.5	20
$XZrTe_{2.5}H$	56	1/3.7	30
$XZrTe_5H$	17	0.7/2.1	28
$XZrTe_{10}H$	11	0.7/1.9	25
$XZrTe_{2.5}H$ 773	−19	0.5/6.3	0

catalytic performance can be explained by the stabilization of suitable active acid sites. These sites should be stabilized by a texture of mesoporosity spaces between parallel plates and morphology of relatively compact particles of a few micrometers size.

However, this is not proportional to the amount of the doping agent because of its low acidity. It seems that the enrichment of catalyst by doping agent only does not increase the number of active acid sites of the esterification reaction, it is necessary that these sites must be stabilized in a mesoporous texture and an adequate morphology.

The study of the catalytic properties of xerogel doped with telluric acid as a function of the calcination temperature reveals that the calcination considerably decreases the catalytic activity and catalyst becomes practically inactive for high calcinations temperature. This can be explained by a considerable drop in the specific surface area and the loss of acidity of the catalyst surface.

3.9 Kinetic, mechanistic, and thermodynamic study of reaction

In this part, we introduce the kinetic and mechanism study of the esterification reaction of acetic acid with benzyl alcohol in the presence of catalyst which exhibits the best catalytic performances.

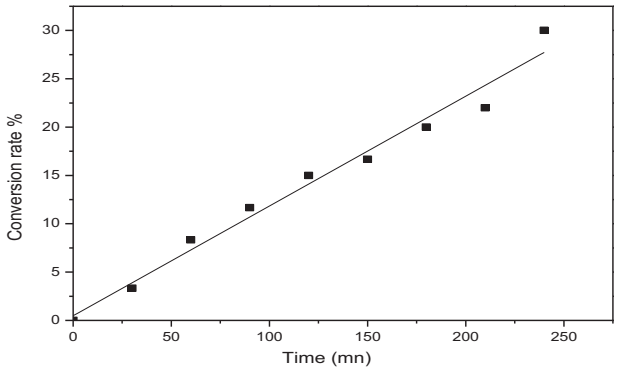

Fig. 12 Conversion rate of acetic acid versus time in the presence of $XZrTe_{2.5}H$. acetic acid:benzyl alcohol, 1:10 (mol/mol); reaction time, 4 h; reaction temperature, 353 K

The kinetics of the catalyzed esterification reaction has been extensively studied. Kirumakki et al. [47] demonstrated that the esterification reaction of acetic acid by benzyl alcohol, in the presence of various zeolites, follows the ER model, with a reaction order equal to 1 with respect to the alcohol. Liu et al. [48] establish that the esterification of oleic acid in the presence of PA/NaY is a pseudo-homogeneous model with a reaction order of 2. Song et al. [49] found that the esterification reaction between oleic acid and methanol catalyzed by Amberlyst 46 resin corresponds to a pseudo-homogeneous second-order model.

Conversion rate of acetic acid vs. time for $XZrT_{2.5}H$ at 353 K was plotted in (Fig. 12).

From the curve, it seems that the conversion varies with versus time. In general, it is observed in heterogeneous solid liquid phase, the diffusion phenomenon outweighs the chemical kinetics. However, it is possible to confirm the order 1 with respect to the acetic acid (Figs. 13 and 14) in our experimental conditions with apparent rate constant $k' = 1.38\ 10^{-3}\ min^{-1}$ at 353 K.

At the level of the reaction mechanism, LH and ER pathways were investigated to propose a reaction

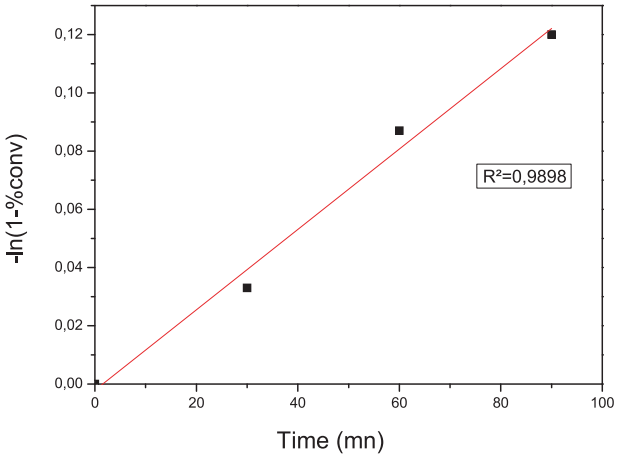

Fig. 13 Plot of -ln (1-% conv) vs. time for the esterification of acetic acid in the presence of $XZrTe_{2.5}H$. acetic acid:benzyl alcohol, 1:10 (mol/mol); reaction time, 4 h; reaction temperature, 353 K

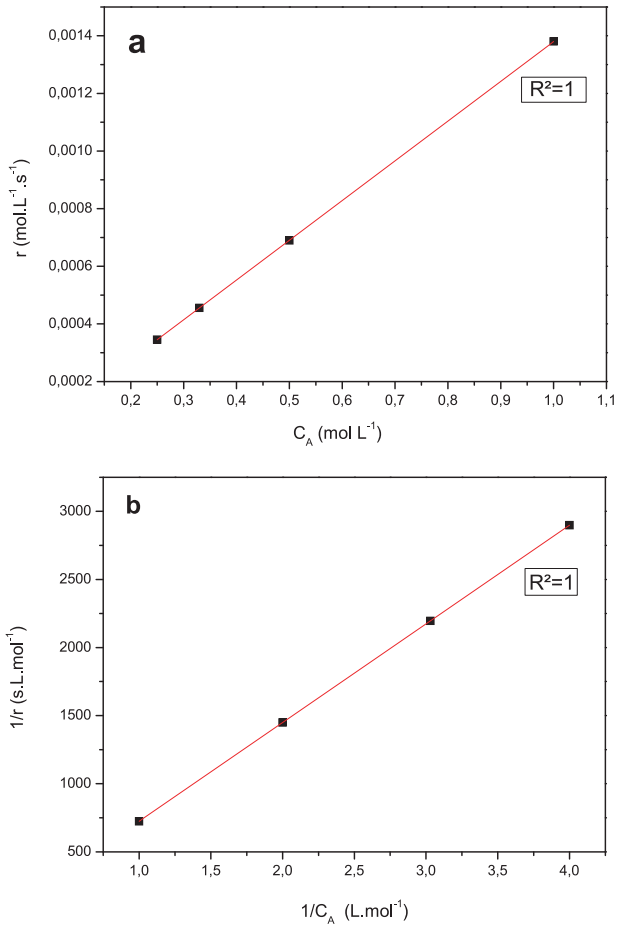

Fig. 14 **a** Curve representing the Eley–Rideal mechanism at the initial state without adsorption. acetic acid:benzyl alcohol, 1:1; 1:2; 1:3; 1:4 (mol/mol). **b** Curve representing the Eley–Rideal mechanism at the initial state with adsorption

Table 5 Rate of the reaction depending on the concentration of acetic acid

Concentration of acetic acid (mol L^{-1})	Reaction rate r (μmol L^{-1} min)
0.25	345
0.33	455
0.5	690
1	1380

mechanism for the esterification of acetic acid with benzyl alcohol over the xerogel catalyst $XZrTe_{2.5}H$.

In the used concentration range (Table 5), the plot of the curve $r = f\ (C_A)$ doesn't exhibit maxima (Fig. 14). Depending to the literature [8], this result suggests that the reaction mechanism does not fit with the LH model, which implies that this reaction follows the ER model. In the initial state, Fig. 14a, b shows that the two possible cases are checked for the esterification reaction, with a correlation factor $R^2 = 1$. This would suggest that benzyl alcohol may be also adsorbed on the same sites as those of acetic acid, but in very small amounts.

To verify this result for a longer time of operating catalyst, these equations were applied for a reaction time of two hours, as indicated in Fig. 15a, b.

In the part of Thermodynamic adsorption characteristics [8], the Eyring expanded equation is:

$$k_{exp} = \frac{k_B \cdot T}{h} \cdot K_{ads} \cdot K^*$$

Where k_{exp} is the rate constant for the reaction, k_B the Boltzmann constant, h the Planck constant, K_{ads} the adsorption equilibrium constant, K^* the Equilibrium constant ($K^* = e^{\frac{-\Delta G^*}{RT}} = e^{\frac{-(\Delta H^* - T\Delta S^*)}{RT}}$).

In this case, apparent activation energy depends on heat adsorption of reactant, while entropy is a factor in determining the pre-exponential factor in the Arrhenius rate equation.

$$K_{exp} = A.e^{\frac{-E_a}{RT}}$$

Both apparent activation energy Ea and the experimental pre-exponential factor A have contributions of adsorption and intrinsic activation steps translated by following relations:

$E_a = \Delta H^0_{ads} + \Delta H^*$ and $\Delta S = \Delta S^0_{ads} + \Delta S^*$

The Fig. 16 allows determining the reaction rate constant at different temperature (Table 6) and calculated Arrhenius parameters are equal to 17.5 kJ mol^{-1} for activation energy with a pre-exponentional factor A = 0.06.

The positive values of $\Delta H^* = 19.2$ kJ mol^{-1} shows the endothermic character [8] of the complex formation and the

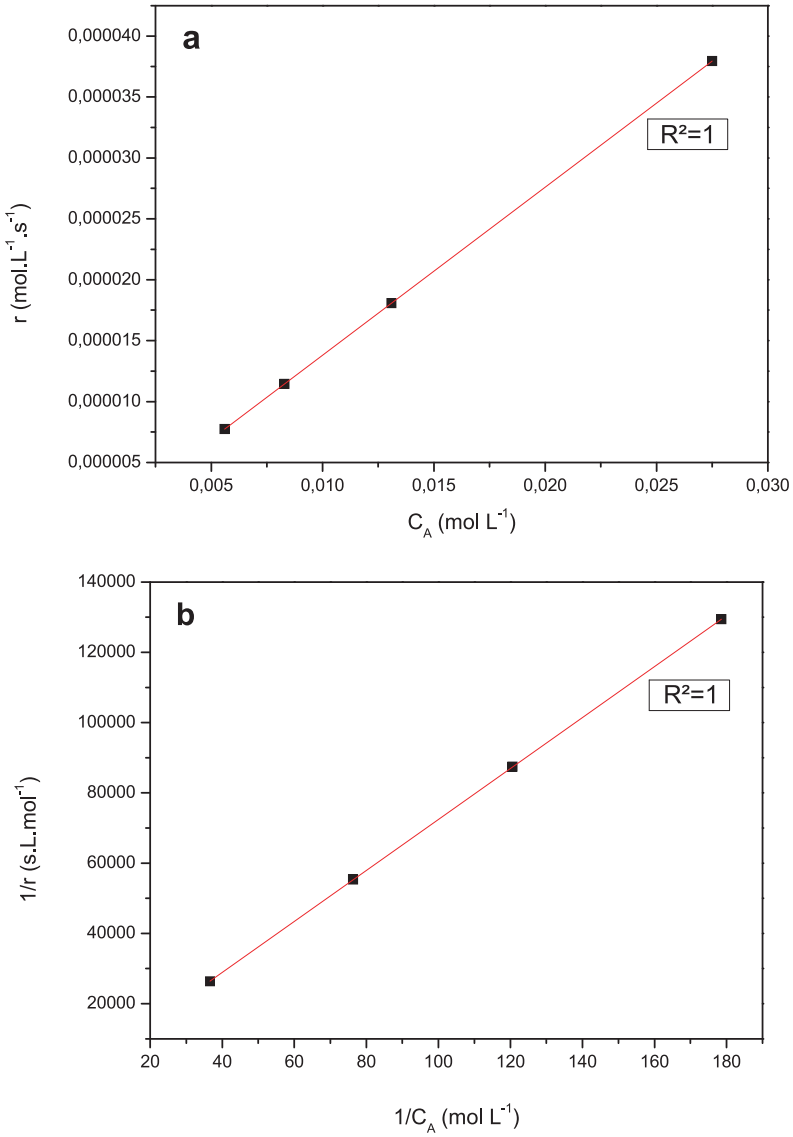

Fig. 15 **a** Curve representing the Eley–Rideal mechanism after two hours of reaction state without adsorption. **b** Curve representing the Eley–Rideal mechanism after two hours of reaction state with adsorption

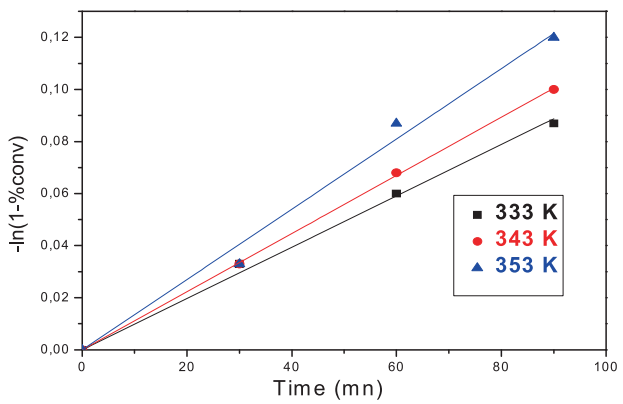

Fig. 16 Plot of –ln(1-%conv) versus time of esterification of acetic acid with benzyl alcohol over $XZrTe_{2.5}H$ at 333, 343, and 353 K

Table 6 Reaction constant at different temperatures

Temperature (K)	k'(10^{-3} min^{-1})	R^2
333	0.96	0.9974
343	1.12	0.99973
353	1.38	0.98981

negative value of $\Delta S^* = -201.7\ J\ mol^{-1}\ K^{-1}$ implies a decrease of disorder thus representing a rapid association step between adsorbed species and second reactant (Fig. 17).

Using values of Ea and ΔH^*, determined previously, ΔH_{ads} of the acid adsorbed step can be estimated as -1.7 kJ mol^{-1}indicating a slightly endothermic adsorption of the acid on the catalyst surface.

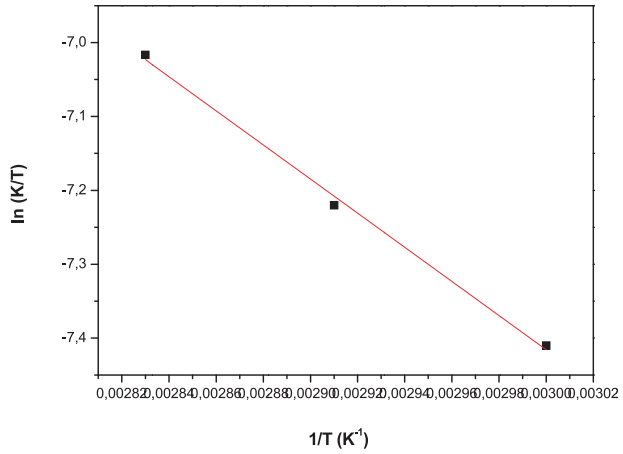

Fig. 17 Plot of ln(k/T) vs. T^{-1} at T = 333, 343, and 353 K

4 Conclusion

The preparation of the telluric acid-doped zirconia xerogel shows that the sol–gel process takes place only if the nitric acid is added to the gelling step. This makes it possible to complete both hydrolysis and condensation reactions. The corresponding catalyst has developed texture and morphology suitable for the stabilization of acidic active sites for esterification of acetic acid by benzyl alcohol. The optimization of the preparation parameters, namely the content of the doping agent and the calcination temperature, shows that the enrichment of the catalyst with the doping agent does not increase its acidity because of its low acidity and that the calcination of the catalyst strongly decreases its acidity by changing its texture and structure and therefore the catalytic reactivity become very low in the studied reaction. Kinetic studies have shown that the esterification follows an ER mechanism.

Acknowledgements Chevreul Institute (FR 2638), Ministère de l'Enseignement Supérieur et de la Recherche, Région Nord-Pas de Calais and FEDER are acknowledged for supporting and funding partially this work. Pardis SIMON is acknowledged for performing the X photoelectron spectrometry experiments of the catalysts.

Funding University of Lille and University of Tunis.

Compliance with ethical standards

Conflict of interest The authors declare no competing interests.

Publisher's note Springer Nature remains neutral with regard to jurisdictional claims in published maps and institutional affiliations.

References

1. Moser BR (2011) Biodiesel production, properties, and feedstocks. Biofuels 285–347
2. Yadav GD, Mehta PH (1994) Heterogeneous catalysis in esterification reactions: preparation of phenethyl acetate and cyclohexyl acetate by using a variety of solid acidic catalysts. Ind Eng Chem Res 33:2198–2208
3. Sharma YC, Singh B, Upadhyay SN (2008) Advancements in development and characterization of biodiesel: a review. Fuel 87:2355–2373
4. Zaidi A, Gainer JL, Carta G (1995) Fatty acid esterification using nylon-immobilized lipase. Biotechnol Bioeng 48:601–605
5. Weissermel K, Arpe H-J (2008) Industrial Organic Chemistry. John Wiley & Sons, Frankfurt, Federal Republic of Germany.
6. Alvarez M, Ortiz MJ, Ropero JL, Niño ME, Rayon R, Tzompantzi F, Gomez R (2009) Evaluation of sulfated aluminas synthesized via the sol-gel method in the esterification of oleic acid with ethanol. Chem Eng Commun 196:1152–1162
7. Corma A, Garcia H, Iborra S, Primo J (1989) Modified faujasite zeolites as catalysts in organic reactions: esterification of carboxylic acids in the presence of HY zeolites. J Catal 120:78–87
8. Nsir SB, Younes MK, Rives A, Ghorbel A (2017) Characterization and reactivity of zirconia-doped phosphate ion catalyst prepared by sol–gel route and mechanistic study of acetic acid esterification by ethanol. J Sol-Gel Sci Technol 84:349–360
9. Parida KM, Pattnayak PK (1996) Studies on PO3− 4/ZrO2: I. effect of H3PO4on textural and acidic properties of ZrO2. J Colloid Interface Sci 182:381–387
10. Hammache S, Goodwin Jr JG (2003) Characteristics of the active sites on sulfated zirconia for N-butane isomerization. J Catal 218:258–266
11. Garcia CM, Teixeira S, Marciniuk LL, Schuchardt U (2008) Transesterification of soybean oil catalyzed by sulfated zirconia. Bioresour Technol 99:6608–6613
12. Ikeda Y, Asadullah M, Fujimoto K, Tomishige K (2001) Structure of the active sites on H3PO4/ZrO2 catalysts for dimethyl carbonate synthesis from methanol and carbon dioxide. J Phys Chem B 105:10653–10658
13. Mejri I, Younes MK, Ghorbel A, Eloy P, Gaigneaux EM (2006) Comparative study of the sulfur loss in the xerogel and aerogel sulfated zirconia calcined at different temperatures: effect on n-hexane isomerization. In: Studies in surface science and catalysis, vol. 162 Elsevier, 953–960 ISBN 0167-2991
14. Hamouda LB, Ghorbel A (2000) Control preparation of sulfated zirconia by sol-gel process: impact on catalytic performances during n-Hexane isomerization. J Sol-Gel Sci Technol 19:413–416
15. Chuah GK, Liu SH, Jaenicke S, Harrison LJ (2001) Cyclisation of citronellal to isopulegol catalysed by hydrous zirconia and other solid acids. J Catal 200:352–359
16. Kamoun N, Younes MK, Ghorbel A, Mamede AS, Rives A (2014) Effect the solvent evacuation mode on the catalytic properties of nickel-modified sulfated zirconia catalysts: N-hexane isomerization. React Kinet Mech Catal 111:199–213
17. Raissi S, Kamoun N, Younes MK, Ghorbel A (2015) Effect of drying conditions on the textural, structural and catalytic properties of Cr/ZrO 2–SO 4: N-Hexane conversion. React Kinet Mech Catal 115:499–512
18. Liquid-Phase Esterification of Propionic Acid with n-Butanol | Industrial & Engineering Chemistry Research. Accessed 4 Dec 2020. https://pubs.acs.org/doi/abs/10.1021/ie001059h
19. Bart HJ, Kaltenbrunner W, Landschützer H (1996) Kinetics of esterification of acetic acid with propyl alcohol by heterogeneous catalysis. Int J Chem Kinet 28:649–656. https://doi.org/10.1002/(SICI)1097-4601(1996)28:9<649::AID-KIN2>3.0.CO;2-V
20. Derouane EG (1998) Zeolites as solid solvents1paper presented at the international symposium 'organic chemistry and catalysis' on the occasion of the 65th birthday of Prof. H. van Bekkum, Delft,

Netherlands, 2–3 October 1997.1. J Mol Catal Chem 134:29–45. https://doi.org/10.1016/S1381-1169(98)00021-1
21. Derouane EG, Crehan G, Dillon CJ, Bethell D, He H, Derouane-Abd Hamid SB (2000) Zeolite catalysts as solid solvents in fine chemicals synthesis: 2. competitive adsorption of the reactants and products in the Friedel–Crafts acetylations of anisole and toluene. J Catal 194:410–423. https://doi.org/10.1006/jcat.2000.2933
22. Villabrille P, Vázquez P, Blanco M, Cáceres C (2002) Equilibrium adsorption of molybdosilicic acid solutions on carbon and silica: basic studies for the preparation of ecofriendly acidic catalysts. J Colloid Interface Sci 251:151–159. https://doi.org/10.1006/jcis.2002.8391
23. El-Sharkawy EA, Khder AS, Ahmed AI (2007) Structural characterization and catalytic activity of molybdenum oxide supported zirconia catalysts. Microporous Mesoporous Mater 102:128–137. https://doi.org/10.1016/j.micromeso.2006.12.037
24. Khder AS, Ahmed AI (2009) Selective nitration of phenol over nanosized tungsten oxide supported on sulfated SnO2 as a solid acid catalyst. Appl Catal Gen 354:153–160. https://doi.org/10.1016/j.apcata.2008.11.030
25. Sing K (1982) Reporting physisorption data for gas/solid systems with special reference to the determination of surface area and porosity. Pure Appl Chem 54:2201–2218. https://doi.org/10.1351/pac198254112201
26. Zhou B, Shen J, Wu Y, Wu G, Ni X (2007) Hydrophobic silica aerogels derived from polyethoxydisiloxane and perfluoroalkylsilane. Mater Sci Eng C 27:1291–1294. https://doi.org/10.1016/j.msec.2006.06.032
27. Moner-Girona M, Roig A, Molins E, Llibre J (2003) Sol-gel route to direct formation of silica aerogel microparticles using supercritical solvents. J Sol-Gel Sci Technol 26:645–649. https://doi.org/10.1023/A:1020748727348
28. Mezza P, Phalippou J, Sempere R (1999) Sol–gel derived porous silica films. J Non-Cryst Solids 243:75–79. https://doi.org/10.1016/S0022-3093(98)00825-4
29. Pattnayak PK, Parida KM (2000) Studies on PO43−/ZrO2: II. Effect of phosphate concentration and activation temperature on the catalytic properties of zirconia. J Colloid Interface Sci 226:340–345. https://doi.org/10.1006/jcis.2000.6822
30. Rodríguez-Castellón E, Jiménez-López A, Maireles-Torres P, Jones DJ, Rozière J, Trombetta M, Busca G, Lenarda M, Storaro L (2003) Textural and structural properties and surface acidity characterization of mesoporous silica-zirconia molecular sieves. J Solid State Chem 175:159–169. https://doi.org/10.1016/S0022-4596(03)00218-4
31. López EF, Escribano VS, Panizza M, Carnasciali MM, Busca G (2001) Vibrational and electronic spectroscopic properties of zirconia powders. J Mater Chem 11:1891–1897. https://doi.org/10.1039/B100909P
32. (PDF) Synthesis and Apparent Bandgap of Nanophase Zirconia. Accessed on 4 Dec 2020. https://www.researchgate.net/publication/227120465_Synthesis_and_Apparent_Bandgap_of_Nanophase_Zirconia
33. Rauta PR, Manivasakan P, Venkatachalam R, Sahu BB, Panda B, Mohapatra P (2012) Phase transformation of ZrO2 nanoparticles produced from zircon. Phase Transit 85:13–26. https://doi.org/10.1080/01411594.2011.619698
34. Sert E, Atalay F (2009) Kinetic study of the esterification of acetic acid with butanol catalyzed by sulfated zirconia. React Kinet Mech Catal 99:125–134. https://doi.org/10.1007/s11144-009-0117-y
35. Altass HM, Khder AERS (2016) Surface and catalytic properties of triflic acid supported zirconia: effect of zirconia tetragonal phase. J Mol Catal Chem 411:138–145. https://doi.org/10.1016/j.molcata.2015.10.022
36. Chakhari S, Younes MK, Rives A, Ghorbel A (2015) Effect of the doping agent nature on the characteristic and catalytic properties of aerogel zirconia catalysts doped with sulfate groups or heteropolytungstic acid. Mater Res Bull 72:35–42. https://doi.org/10.1016/j.materresbull.2015.07.012
37. Raissi S, Younes MK, Ghorbel A, Garin F (2010) Effect of sulphate groups on catalytic properties of chromium supported by zirconia in the N-hexane aromatization. J Sol-Gel Sci Technol 53:412–417
38. Kamoun N, Younes MK, Ghorbel A, Mamede A-S, Rives A (2015) Comparative study of aerogels nanostructured catalysts: Ni/ZrO 2–SO 4 2− and Ni/ZrO 2–Al 2 O 3–SO 4 2−. Ionics 21:221–229
39. Dong Y, Qi L, Li J, Chen I-W (2017) A computational study of yttria-stabilized zirconia: II. Cation diffusion. Acta Mater 126:438–450. https://doi.org/10.1016/j.actamat.2017.01.008
40. Crist BV (1999) Handbook of the Elements and Native Oxides. XPS Int. Inc, Iowa USA
41. Chen X, Yang Q, Chu B, An H, Cheng Y (2015) Valence variation of phase-pure M1 MoVNbTe oxide by plasma treatment for improved catalytic performance in oxidative dehydrogenation of ethane. RSC Adv 5:91295–91301
42. Chowdari BVR, Pramoda Kumari P (1996) Thermal, electrical and XPS studies of Ag2O·TeO2·P2O5 glasses. J Non-Cryst Solids 197:31–40. https://doi.org/10.1016/0022-3093(95)00548-X
43. Tesfaye F, Sukhomlinov D, Lindberg D, Taskinen P, Akdogan G (2017) Thermal stabilities and properties of equilibrium phases in the Pt-Te-O system. J Chem Thermodyn 106:47–58. https://doi.org/10.1016/j.jct.2016.11.016
44. Mendes MK, Martinez E, Marty A, Veillerot M, Yamashita Y, Gassilloud R, Bernard M, Renault O, Barrett N (2018) Forming mechanism of Te-based conductive-bridge memories. Appl Surf Sci 432:34–40
45. Rafiee E, Joshaghani M, Abadi PG-S (2019) Synthesis and characterization of carbon@ HPW core/shell nanorod using potato as a novel precursor: efficient catalyst for CN coupling reaction. Arab J Chem 12:3324–3335
46. Tanabe K, Misono M, Hattori H, Ono Y (1990) New solid acids and bases: their catalytic properties. Elsevier, Amsterdam-Oxford-New York-Tokyo
47. Kirumakki SR, Nagaraju N, Narayanan S (2004) A comparative esterification of benzyl alcohol with acetic acid over zeolites Hβ, HY and HZSM5. Appl Catal Gen 273:1–9
48. Liu W, Yin P, Zhang J, Tang Q, Qu R (2014) Biodiesel production from esterification of free fatty acid over PA/NaY solid catalyst. Energy Convers Manag 82:83–91
49. Song C, Qi Y, Deng T, Hou X, Qin Z (2010) Kinetic model for the esterification of oleic acid catalyzed by zinc acetate in subcritical methanol. Renew Energy 35:625–628